CrystEngComm

Photoluminescent chromium molybdate cluster coordinated with rare earth cations: Synthesis, structure, optical and magnetic properties

Journal:	*CrystEngComm*
Manuscript ID:	CE-ART-04-2014-000865.R1
Article Type:	Paper
Date Submitted by the Author:	01-Jun-2014

Complete List of Authors:	Kumar, Dinesh; IIT Delhi, Department of Chemistry Ahmad, Shahab; IIT Delhi, Physics Dept Prakash, G. Vijaya; IIT Delhi, Physics Dept Ramanujachary, Kandalam; Rowan University, Chemistry and Biochemistry Arunachalam, Ramanan; IIT Delhi India, chemistry

Cite this: DOI: 10.1039/c0xx00000x

www.rsc.org/xxxxxx

ARTICLE TYPE

Photoluminescent chromium molybdate cluster coordinated with rare earth cations: Synthesis, structure, optical and magnetic properties

Dinesh Kumar[a], Shahab Ahmad[b], G.Vijaya Prakash[b*], Kandalam V. Ramanujachary[c] and Arunachalam Ramanan[a*]

Received (in XXX, XXX) Xth XXXXXXXXX 20XX, Accepted Xth XXXXXXXXX 20XX
DOI: 10.1039/b000000x

ABSTRACT: Anderson-Evans cluster, $\{CrMo_6O_{24}\}^{n-}$ exhibits ruby–like red emission. During our attempts to engineer new photoluminescent crystals using the chromium molybdate as a molecular building block, we isolated four new rare–earth based chromium molybdates: $[Gd(H_2O)_7\{CrMo_6(OH)_6O_{18}\}].4H_2O$ **1**, (4–*pycH*)$[Gd(H_2O)_4\{CrMo_6(OH)_6O_{18}\}$(4–*pycH*)].$5H_2O$, **3** and (4–*pycH*)$_2[Ln(H_2O)_6\{CrMo_6(OH)_6O_{18}\}].2H_2O$, (Ln= Tb, **4** and Sm, **5**; 4–*pyc* = 4–pyridine carboxylate and 4–*pycH* =4–pyridinium carboxylate). All are nonmolecular solids characterized by extended 1-D or 2-D interaction between rare-earth ions and the chromium molybdate cluster. All solids showed intense room-temperature Cr^{3+} related red emission and also exhibited weak antiferromagnetism at low-temperatures.

Introduction

Anderson–Evans cluster anion, $\{CrMo_6O_{24}\}^{n-}$ is a well-known cluster that occurs as a building block in several polyoxomolybdate based solids.[1] The disk-shaped cluster is a versatile ligand as its peripheral oxygen atoms are potential centers to assemble into multidimensional structures with appropriate molecules either through H–bonding or metal–ligand interaction or both (Tables S1 and S2).[2] In this cluster, chromium(III) occurs in a pseudo–octahedral coordination, made of six oxygen ligands in a trigonally distorted symmetry. The cluster exhibits red emission and is considered as molecular equivalent of the much studied fluorophore namely ruby (chromium doped alumina).[3] The unique photoluminescent behavior of the Anderson–Evans cluster, $[H_xCrMo_6O_{24-x}]^{n-}$ was first investigated by Yamase and his group[4] almost two decades ago. Since then, the molecular cluster was crystallized in the presence of a variety of complex cations exploiting its stability in aqueous solution over a large pH window and its coordinating ability with transition and rare–earth metal ions.[5] Surprisingly, there are only a few reports on the photoluminescent properties of solids built on this versatile molecule.[4] During our investigation on Anderson–Evans cluster based solids,[6] we observed that single crystals made of chromium molybdate clusters were light to dark purple in color. Our preliminary investigation of its optical properties revealed that in most cases the color of the solids was dominated by a red emission reminiscent of ruby. All our earlier studies involved only transition metal ions (Fig. S1).[6] The results prompted us to investigate photophysical properties of chromium molybdates coordinated with rare–earth ions which are potential emitters. CSD analysis[7] of Anderson-Evans cluster based solids containing rare-earth cations showed that there were twenty solids reported in the literature. Majority of the solids can be broadly classified into four categories based on the interactions between rare-earth ions and chromium molybdates cluster (Table S3). Our objective was to isolate new solids and investigate its optical and magnetic properties.

In this paper, we report crystallization of four new solids built of Anderson–Evans cluster coordinated with selected rare–earth ions. All the crystals are strongly photoluminescent and exhibit only ruby–like fluorescent behavior; the rare–earth ions were silent with no characteristic emission. Apart from structurally characterizing these solids using single crystal X–ray diffraction and other thermal and spectroscopic techniques, we have also reported its low temperature magnetic properties

Experimental Section

All reagents were used as received from commercial sources without further purification. We adopted a synthetic protocol similar to the one employed in our earlier studies.[6] In a few cases, the procedure was slightly modified to obtain good crystals for diffraction experiments. Rietveld analysis of powder diffraction patterns were performed to ascertain the monophasic nature of the solids obtained.

Initially two different aqueous solutions were prepared. The experimental conditions were optimized to enable homogeneity of the solution before and after mixing. Solution A was prepared by mixing $LnCl_3.6H_2O$ (Ln= Gd, 1.34 mmol for **1** and **3**, and Sm, 1.372 mmol for **2**) and H4–*pyc* (2.68 mmol, only for **1** and **3**) in 10 mL of water and 10 mL of methanol. Solution B was prepared by adding $CrCl_3.6H_2O$ (1.53 mmol) to $Na_2MoO_4.2H_2O$ (2.356 mmol) in 15 mL of H_2O and further acidified by 7 mL of glacial acetic acid. Solution A was then added to solution B with stirring. The resulting dark green colored solution was refluxed at 80^0C for three to four hours for solids **1** and **3;** the solid **2** was isolated when the appropriate solution was refluxed at 80^0C for 30 min (Scheme 1). Purple color crystalline products of **1**, **2** and

3 were grown at room temperature (Yield: ca. 40–50 % based on Mo for **1, 2** and **3**). Similar experimental condition yielded block purple crystalline solid **4** ($TbCl_3.6H_2O$ (0.335 mmol) with H4–*pyc* (0.935 mmol) and solid **5** was obtained with $SmCl_3.6H_2O$ in place of $TbCl_3.6H_2O$ (0.343 mmol) (Yield: ca. 40–50 % based on Mo for both **4** and **5**). Both **4** and **5** obtained at refluxed 80^0C for 30 min.

Physical Measurement

TG analyses were carried out using Perkin–Elmer TGA7 system on well ground samples in flowing nitrogen atmosphere with a heating rate of 10 °C/min with range 50–1000ºC. ATR–FTIR was recorded on a Perkin–Elmer spectrometer. The susceptibility measurements as a function of temperature were performed with a SQUID magnetometer of Quantum Design Inc. USA. Diamagnetic corrections were estimated from Pascal's constants.[8]

X-ray crystallographic studies

X–ray diffraction study of a crystal mounted on a capillary was carried out on a BRUKER AXS SMART–APEX diffractometer with a CCD area detector (Kα: 0.71073 Å, monochromator: graphite).[9] Frames were collected at T = 298 K by ω, ϕ and 2θ – rotation at 10 s per frame with SAINT.[10] The measured intensities were reduced to F^2 and corrected for absorption with SADABS.[10] Structure solution, refinement, and data output were carried out with the SHELXTL program.[11] Non–hydrogen atoms were refined anisotropically. C–H hydrogen atoms were placed in geometrically calculated positions by using a riding model. Images were created with the DIAMOND program.[12] Hydrogen bonding interactions in the crystal lattice were calculated with SHELXTL and DIAMOND.[11, 12] The crystal data and structure refinement for solids **1** and **3**–**5** are summarized in Table 1. Rietveld powder diffraction analysis of **1**, **3**, and **4** were carried out using Topas 4.2, Bruker[13] for ensuring homogeneity of the synthesized products (Fig. S2).

Optical measurement

The room–temperature photoluminescence (PL) spectra and crystal PL imaging measurements were performed using a confocal microscope (Olympus BX–51) equipped with 410nm diode laser and white light xenon lamp source. The spectra have been recorded using Ava spec CCD based spectrometer connected with the microscope through optical fibre. All PL spectra, conventional confocal bright field images and PL images were recorded using an ALP >425 nm filter. The time–resolved photoluminescence (PL) measurements were carried out using home–built setup with 410 nm (diode laser) as the excitation source. The emission was dispersed into a monochromator coupled to a photo multiplier tube (PMT) through select appropriate lenses and filters. For time–resolved photoluminescence, a square wave pulse–function generator (12 Hz), lock–in amplifier and digital storage oscilloscope were employed. The photoluminescence excitation spectrum (PLE) has been recorded by using commercial flourimeter (Shimadzu RF–5301PC). Diffuse–reflectance was recorded using Perkin–Elmer Lambda 1050 spectrophotometer.

Results and Discussion

Crystal structures of rare–earth coordinated Anderson–Evans cluster based solids, 1–5

Crystallization under our experimental condition led to the isolation of five solids **1**–**5** containing chromium molybdate cluster coordinated to gadolinium, samarium and terbium ions. The molecular structure of chromium molybdates cluster, $\{CrMo_6O_{24}\}$ in all the five solids is identical to those already reported by us as well as in the literature.[1] The gadolinium based solids **1** and **3** were isolated under different refluxing condition of the initial solution (Scheme 1). In $[Gd(H_2O)_7\{CrMo_6(OH)_6O_{18}\}].4H_2O$ **1**, Gd atoms are coordinated to the cluster forming extended 1-D zig–zag chains as shown in Fig. 1. The chains are further H–bonded to each other through lattice water molecules. The solid **2**, a samarium analogue of **1** (Fig. S3) is already known but prepared by a different route.[14] Till now, only three isostructural solids are known[14] with the composition, $[Ln(H_2O)_7\{CrMo_6(OH)_6O_{18}\}].4H_2O$, Ln=Ce, Sm and Eu; solid **1** reported in this study is the fourth member. In (4–*pycH*)$[Gd(H_2O)_4\{CrMo_6(OH)_6O_{18}\}$(4–*pycH*)$].5H_2O$ **3,** the structure is built of three main building blocks: A gadolinium dimer bridged by a pair of 4–*pycH*, the chromium molybdate cluster and the zwitterionic 4–pyridine carboxylic acid. Each gadolinium dimer is coordinated through four POM clusters (Fig. 2) forming a double stranded sheet parallel to *ab*–plane; the disc shaped clusters lie on the sheets while the Gd dimers occur in between them. The double stranded sheets are further strengthened by zwitterionic 4–pyridine carboxylic acid through H–bonding (Fig. 2). Along the *c*–axis, the cluster molecules on adjacent strands are also connected through H–bonding. In addition, the cavities between the sheets contain hexameric water clusters that are further linked by lattice water H–bonded to cluster oxygens (Fig. 2). This compound is a fifth member of the isostructural series of rare-earth (La, Ce, Pr and Nd) coordinated Anderson-Evans cluster based solids.[15] Single crystal structure of $(4–pycH)_2[Tb(H_2O)_6\{CrMo_6(OH)_6O_{18}\}].2H_2O$ (**4)** showed Tb atoms are coordinated to the clusters forming extended neutral 1-D chains similar to **1** and **2**. A pair of chains is linked by zwitterionic 4–pyridine carboxylic acid through H–bonding forming sheets along *ab* plane. In addition, there is also C─H···л interaction between two zwitterionic 4–pyridine carboxylic acid strengthening the crystal structure (Fig. 3). The samarium analogue **5** is a new solid and is isostructural to **4** (Fig. S4).

CSD analysis (Table S1) of all rare–earth coordinated chromium molybdates suggested that quite often the coordination behaviour of the metal with the cluster is similar and results in isostructures; this is in contrast to transition metal based solids.[6] The structural chemistry is dominated by the occurrence of extended 1-D interaction between rare-earth and the cluster. Majority of the solids can be broadly classified into four categories: (i) rare-earth hydrate coordinates the cluster to form neutral chains; further stabilization of the chains is facilitated through H-bonding either by lattice water or organic and water. The structure of solids **1**, **2**, **4** and **5** reported here come under Class I category. Under certain crystallization condition, the rare-earth can form dimers through bridging organic ligands. This building block favors 2-D interaction to form sheets which is shown by Class II solids; **3** is an example of this kind. Class III is

a unique type of solids where rare-earth interacts with the cluster in 3-D. Only two examples are known in the literature (Table S3). The fourth class comes under the category of molecular solids wherein the rare-earth complexes aggregate with the cluster through H-bonding interactions; in this category there is no direct coordination between rare-earth ion and the cluster (Table S3). The structural features may be of importance with respect to the photophysical properties of the solids discussed later.

Thermal decomposition studies and vibrational spectroscopy

Solids **1** and **3**–**5** show complex dehydration and decomposition behaviour. All the solids became amorphous after heating above 300^{o}C **(**Fig. S5). AT–FTIR for solids **1** and **3**–**5** showed absorptions characteristic of Anderson–Evans cluster type structure reported earlier,[4] the region between 890 and 950 cm^{-1} correspond to Mo–Ot bonds, 650 and 800 cm^{-1} from Mo–Ob groups, and 400 and 600 cm^{-1} due to Mo–Oc units. The bands around 1570 and 1645 cm^{-1} are due to the presence of C=O of carboxylate ion and C=O of carboxylic acid (H–bond) in solids **3** and **4**, **5 (**Fig. S6) respectively.

Optical Properties of rare-earth coordinated chromium molybdates

The optical properties of the chromium (III) based rare–earth molybdates have been studied to understand the absorption and emission characteristics. The photoluminescence (PL) studies of all crystals (solid **1**–**5**) were performed at room temperature by exciting single crystals with low power 410nm diode laser; we also recorded photoluminescence of the reference sample, $[\{Na_3(H_2O)_{11}\}\{CrMo_6O_{18}(OH)_6\}].2H_2O$, **6** in powdered form as suitable single crystals were unavailable.[16] All crystalline solids exhibit strong reddish–purple colour emission and corresponding spectra are shown in Fig. 4a. For comparison, we have given the corresponding white–light reflection (bright field) images and PL images (λ_{ex}~410nm; collected using appropriate long pass filter) for all the crystals (**1**–**5**) and the powder sample of **6** in Fig. 4b. The excitation and emission spectra for one of the solids is shown in Fig. 5a as representative one. The prominent photoluminescent excitation (PLE) transitions at 423, 581 and 648nm correspond to absorption transitions of Cr^{3+} ions, $^4A_2 \rightarrow {}^4T_1(F)$, $^4T_2$ and $^2T_1$ (denoted by blue lines). Similarly the emission transitions occurring at around 692, 709 and 733nm are attributed to Cr^{3+} ion transitions of stokes shifted $^2T_1 \rightarrow {}^4A_2$ [R–lines] and $^2E \rightarrow {}^4A_2$ transitions respectively (denoted by red lines). It is widely accepted that Cr^{3+} ion emission is highly dependent on temperature and the matrix in which the ion is situated.[4] The schematic illustration of Cr^{3+} ion energy levels[3] in the present matrix is represented in Fig. 5d. T. Yamase and M. Sugeta reported Cr^{3+} ion in $Na_3H_6[CrMo_6O_{24}].8H_2O$ showed sharp emissions around 703 and 704.4nm at 4.2K and assigned it to R-lines.[4] In these Anderson cluster-based solids, the emission quantum yields of R-lines are extremely low, even at low-temperature, probably due to strong non-radiative deactivation process from Cr^{3+} ion sites to that of $Cr(OH)_6$ sites. However, in all our studied complexes, the room-temperature studies demonstrate remarkable reddish emission (Fig 4, PL images), even visible to naked eye, suggesting that the aforementioned non-radiative process is ineffective. It is further interesting to note that even though the solids **2**, **5** and **4** contains strong visible light–emitting rare–earth ions namely Sm^{3+} and Tb^{3+}, we did not observe any characteristic emissions from these ions as seen in the literature.[17] One of the characteristic feature of trivalent rare–earth ion is the strong and sharp 4f shell absorption and emissions, that covers wide range of spectral region, from ultraviolet (UV) to infrared region.[18] Further the rare–earth 4f–4f transition strengths and positions are sensitive to the local environment within a crystalline network. In the visible spectral region, Tb^{3+} ions usually shows strong green emission at ~544nm corresponding to $^5D_4 \rightarrow {}^7F_5$ along with other ^7F_J lines whereas Sm^{3+} exhibits red emission at ~599nm corresponding to $^4G_{5/2} \rightarrow {}^6H_{7/2}$ transitions. However, in the present case, the observed emission is essentially from Cr^{3+} without any traces of contribution from rare–earth. This is further verified by observing emission with various UV excitation wavelengths and also rare–earth independent sample (solid **6**). The suppression of rare–earth emission and dominant chromium emission could be attributed to a strong absorption cross-section of Cr^{3+} ions and a strong energy transfer (ET) between 4f–4f emission transitions of Sm^{3+} (or Tb^{3+}) ion to that of Cr^{3+} d–orbital energy levels. The possible ET is between the $^4F_{7/2}$ to $^4T_1$(F) and $^5D_3$,$^5D_7$ to $^4T_1$(F) for Sm^{3+} and Tb^{3+} respectively.[19] The cross relaxation between Sm^{3+} (or Tb^{3+}) to Cr^{3+} probably involves the following mechanism.

$^6H_{5/2}$ (Sm^{3+}) +$^4A_2$ (Cr^{3+}) → $^4F_{7/2}$ (Sm^{3+})+$^4T_1$ (F) (Cr^{3+})

$^7F_6$ (Tb^{3+}) +$^4A_2$ (Cr^{3+}) ⟶ $^5D_3$,$^5D_7$ (Tb^{3+})+$^4T_1$ (F) (Cr^{3+})

As an example, the PL decay time of prominent 692nm Cr^{3+} emission has also been recorded for solid **5**. The single exponential PL decay (Fig. 5c) estimates the life time of ~240 μsec which is in close agreement with the values reported for other Cr^{3+} organic complexes.[20] Further, the PL and PLE spectra recorded for aqueous solutions of the bench mark solid, $[\{Na_3(H_2O)_{11}\}\{CrMo_6O_{18}(OH)_6\}].2H_2O$, **6** showed that Cr^{3+} ion emission is similar in both solid and solution state (Fig. 5b). In general, the crystal emission spectra show more discrete and narrow transitions compared to the solution phase due to the well–known phenomena of crystal field effects.[18]

Shi et al[14] reported photoluminescent property of the europium analogue of **1**; surprisingly this solid showed only characteristic emissions due to europium ions and no trace of Cr^{3+} emissions. A molecular solid (0-D) based on dysprosium, chromium molybdate and 4-pyridine carboxylic acid (Class IV) showed characteristic emission only from Dy^{3+} ion,[5] in this case there is no direct coordination between rare-earth and cluster. Further work is in progress to examine the photoluminescent behavior of both emitters in all the four classes of solids wherein the metal−ligand interaction varies in dimensionality.

Electronic spectra

Reflectance spectra of the solids **1**–**4** and **6** (Fig. S7) showed characteristic absorptions $^4A_2 \rightarrow {}^4T_2$ and $^4T_1$ around 546 and 400 nm similar to earlier report.[4]

Magnetic Properties

The temperature–dependent magnetic susceptibilities of **1**, **3** and **4** were recorded over a range of 300–3K. χ_M is the molar magnetic susceptibility corrected for the diamagnetic contribution. The plots of $\chi_M T$ and χ_M versus T of **1**, **3** and **4** are shown in Fig. 6. $\chi_M T$ value is practically constant at temperatures > 100 K and may be compared with the calculated values using the equation based on the free-ion approximation,

$\chi_M T=(N_A\beta^2/3k).[g_{Cr(III)}{}^2 S_{Cr(III)}(S_{Cr(III)}+1)+g_{JTb(III)}{}^2 J_{Tb(III)}(J_{Tb(III)}+1)]$

where N_A is the Avogadro number, β the Bohr magneton and k the Boltzmann constant; it is assumed that the two spin centers do not interact. The g-factors for chromium ($g_{Cr(III)}$ = 2.0) and terbium (g_J = 1.5) are taken from the literature.[21] The calculated and observed values (T = 300 K) for $\chi_M T$ are given in table 2. The experimental $\chi_M T$ at room temperature for solids **1** and **3** are closer to the calculated values based on the above equation though the value is slightly higher in the case of **3**. However, for solid **4** the experimental value is slightly lower.

The magnetic susceptibility data of **1**, **3** and **4** obey the Curie–Weiss law, $\chi_M = C/(T-\theta)$ (C = 10.63 emu mol^{-1}.K, θ= –3.78 K for **1**; C = 11.50 emu mol^{-1}.K, θ = –4.50 K for **3** and C = 13 emu mol^{-1}.K, θ= –3.30 K for **4**). The small Weiss constants suggest the possibility of weak antiferromagnetic interaction between the neighbouring spins.[22]

Conclusion

We have successfully employed metal−ligand interactions to engineer 1-D (Class I) or 2-D (Class II) rare-earth coordinated chromium molybdates. All the solids exhibit photoluminescent property essentially due to chromium molybdates cluster with no significant emission from the rare–earth ions. It is suggested that investigation of the photophysical properties of more solids with these two emitters interacting in different dimensions may throw light on their nature and probably the presence/absence of one or the other. In the context of crystal engineering, the chromium molybdate cluster is a potential molecular building block to explore new solids with promising photophysical properties.

Acknowledgements

D.K. acknowledges DST, Government of India for a research fellowship and S.S. Jyothirmayee from Rowan University for magnetic characterization. Authors are thankful to Prof. Toshihiro Yamese from Tokyo Institute of Technology, Japan for his help in the discussions. A.R. acknowledges DST for financial support as well as the X–ray diffraction facility (Powder and Single Crystal Diffractometer) to the Department of Chemistry, IIT Delhi. This work is part funded by the projects from DST, Govt. of India and High–Impact Research grant of IIT Delhi.

Supporting Information Available

Crystallographic information files (CIF) for solids **1** and **3**–**5**. Chromium Anderson-Evans cluster based solids reported in the literature (Table S1 and S2). Anderson–Evans cluster, $[H_mCrMo_6O_{24}]^{n-}$ based solids reported earlier from our lab (Fig. S1). Structural classification of Ln-$[CrMo_6O_{24}]^{n-}$ system (Table S3). Rietveld analysis of the powder diffraction data of **1**, **3** and **4** (Fig. S2). Crystal packing of 1-D supramolecular solids **2** and **5** (Fig. S3 and S4). TG/DT plots for solids **1**, **3**, **4** and **5** in nitrogen atmosphere (Fig. S5). ATR–FTIR spectra of solids **1**, **3**, **4** and **5** (Fig. S6). Diffused reflectance of solids **1**–**4** and **6** (Fig. S7).

Notes and references

[a] *Department of Chemistry, Indian Institute of Technology Delhi, Hauz Khas, New Delhi-110016, India. Fax: +91-11-26581102; Tel: +91-11-26581507; E-mail: aramanan@chemistry.iitd.ac.in*

[b] *Nanophotonics Lab, Department of Physics, Indian Institute of Technology Delhi, Hauz Khas, New Delhi 110016, India*

[c] *Department of Chemistry and Biochemistry, Rowan University, Glassboro, New Jersey 08028, USA*

† *Electronic Supplementary Information (ESI) available:* [details of any supplementary information available should be included here].

1 A. Saad, G. Rousseau, H. E. Moll, O. Oms, P. Mialane, J. Marrot, L. Parent, I. –M. Mbomekalle, R. Dessapt and A. Dolbecq, *J. Cluster Sci*., 2014, **25**, 795; C.-H. Zhang, C.-J. Zhang and Y.-G. Chen, *Solid State Sci.*, 2011, **13**, 1122; R.–K. Tan, S.–X. Liu, W. Zhang, S.–J. Li and Y.–Y. Zhang, *Inorg. Chem. Comm.*, 2011, **14**, 384; R. Ran, H. Pang, Z. Yu, H. Ma and Y. Xun, *J. Coord. Chem.,* 2011, **64**, 2388; H. An, X. Liu, H. Chen, Z. Han, H. Zhang and Z. Chen, *CrystEngComm*, 2011, **13**, 5384; Q. Wu, W.-L. Chen, D. Liu, C. Liang, Y.-G. Li, S.-W. Lin and E. Wang, *Dalton Trans.,* 2011, **40**, 56.

2 H. An, Y. Li, E. Wang, D. Xiao, C. Sun and L. Xu, *Inorg. Chem.,* 2005, **44**, 6062; A. Perloff, *Inorg. Chem.* 1970, **9**, 2228; S. Golhen, L. Ouahab, D. Grandjean and P. Molinie, *Inorg. Chem*. 1998, **37**, 1499; An, H.; Y. Guo, Y. Li, E. Wang, J. Lu, L. Xu and C. Hu, *Inorg. Chem. Commun.* 2004, **7**, 521; Y. Wang, D. Xiao,Y. Qi, E. Wang, J. Liu, *J. Cluster Sci.* 2008, **19**, 367; P.-P. Zhang, J. Peng, A.-X. Tian, J.-Q. Sha, H.-J. Pang, Y. Chen, M. Zhu and Y.-H. Wang, *J. Mol. Struct*. 2009, **931**, 50; S. Zhang, Y. Li, Y. Liu, R. Cao, C. Sun, H. Ji and S. Liu, *J. Mol. Struct*. 2009, **920**, 284; R.-G. Cao, S.-X. Liu, Y. Liu, Q. Tang, L. Wang, L.-H. Xie and Z.-M. Su, *J. Solid State Chem*. 2009, **182**, 49; V. Shivaiah and S. K. Das, *Inorg. Chem*. 2005, **44**, 8846; H.-Y. Ma, L.-Z. Wu, H.-J. Pang, X. Meng and J. Peng, *J. Mol. Struct*. 2010, **967**, 15; Y.-Y. Yang, Y. Song, L.-Y. Liu, X.-S. Qu, *Acta Cryst.*, 2011, **E67**, m776; S.-M. Wang, Y.-W. Li, X.-J. Feng, Y.-G. Li and E. B. Wang, *Inorg Chim Acta,* 2010, **363**, 1556.

3 K. Hermanowicz, J. Hanuza, M. Maczka, P. J. Deren, E. Mugenski, H. Drulis, I. Sokolska and J. Sokolnicki, *J. Phys.: Condens. Matter,* 2001, **13**, 5807; S. V. J. Lakshman and P. R. Devi, *Proceedings of the Indian National Science Academy, Part A: Physical Sciences,* 1979, **45**, 352; J. A. Duffy, *Bonding, Energy Levels and Bands in Inorganic Solids*; John Wiley and sons, Inc.: New York, 1990.

4 T. Yamase and M. Sugeta, *J. Chem. soc. Dalton Trans.,* 1993, **5**, 759; I. Takeru, Y. Hisashi and T. Yamase, *Langmuir,* 2006, **22**, 2806.

5 L. Yang, Z. Zhou, P.–T. Ma, X.–F. Zhang, J.–P. Wang and J.–Y. Niu, *J. Coord. Chem.,* 2013, **66**, 1058; Y. Liu, S.–X. Liu, R.–G. Cao, H.–M. Ji, S.–W. Zhang and Y–H. Ren, *J. Solid State Chem.,* 2008, **181**, 2237; R. Cao, S. Liu, L. Xie, Y. Pan, J. Cao and Y. Liu, *Inorg. Chim. Acta,* 2008, **361**, 2013; A. B. Yusova, M. Yinb, A. M. Fedosseeva, G. B. Andreeva, I. B. Shirokovaa and J.–C. Krupab, *J. Alloys Compd.,* 2002, **344**, 289; H. An, D. Xiao, E. Wang, C. Sun, Y. Li and L. Xu, *J. Mol. Struct*., 2005, **751**, 184.

6 M. Singh, D. Kumar and A. Ramanan, *Proc. Natl. Acad. Sci., India, Sect. A Phys. Sci.,* 2014 (DOI 10.1007/s40010–014–0144–6); M. Singh and A. Ramanan, *Cryst. Growth Des.,* 2011, **11**, 3381; M. Singh, S. E. Lofland, K.V. Ramanujachary and A. Ramanan, *Cryst Growth Des.*, 2010, **10**, 5105; K. Pavani, M. Singh and A. Ramanan, Aust. J. Chem., 2011, **64,** 68; M. Singh, *Crystal engineering of Metal Complex or Coordination Polymer templated Polyoxomolybdates: Chemical Insights,* Ph.D. Thesis, Indian

Institute of Technology Delhi, India, October 2011; K. Pavani, *Transition Metal Complex Templated Polyoxomolybdates: Synthesis, Structure and Magnetism*, Ph.D. Thesis, Indian Institute of Technology Delhi, India, August 2007.

7 Cambridge Structural Database System; Cambridge Structural Database: Cambridge, UK, 2013.

8 Olivier, K. *Molecular Magnetism*; VCH Publishers, Inc.: New York, 1993.

9 Bruker Analytical X–ray Systems, SMART: Bruker Molecular Analysis Research Tool, Version 5.618; Bruker AXS: Madison, WI, 2000.

10 Bruker Analytical X–ray Systems, SAINT–NT, Version 6.04, Bruker AXS: Madison, WI, 2001.

11 Bruker Analytical X–ray Systems, SHELXTL–NT, Version 6.10; Bruker AXS: Madison, WI, 2000.

12 B. Klaus, DIAMOND, Version 1.2c; University of Bonn: Germany, 1999.

13 TOPAS V4.2: General Profile and Structure Analysis Software for Powder Diffraction Data, Bruker AXS GmbH, Karlsruhe, Germany, 2009.

14 D.–M. Shi, F.–X. Ma, C.–J. Zhang, S. Lu and Y.–G. Chen, *Z. Anorg. Allg. Chem.,* 2008, **634**, 758.

15 H. An, D. Xiao, E. Wang, Y. Li and L. Xu, *New J. Chem.*, 2005, **29**, 667.

16 L. Yu, S.-Z. Li and J.-P. Wang, *Acta Cryst.,* 2006, **E62**, i190.

17 P. Wang, R.–Q. Fan, Y.–L. Yang, X.–R. Liu, P. Xiao, X.–Y. Li, W. Hasi and W.–W. Cao, *CrystEngComm,* 2013, **15**, 4489.

18 R. Reisfeld and C. K. Jorgensen, *Lasers and excited states of rare earths*; Springer Berlin Heidelberg, New York, 1977.

19 K. Swapna, S. k. Mahamuda, A. S. Rao, S. Shakya, T. Sasikala, D. Haranath, and G. V. Prakash, *Spectrochim. Acta A,* 2014*,* **225**, 53; S. Ahmad, S. Das, R. Nagarajan and G.V. Prakash, *Opt. Mater.,*2013*,* **36**, 396; A. A. Reddy, S. Das, A. Goel, R. Sen, R. Siegel, L. Mafra, G. V. Prakash, and J.M.F. Ferreira, *AIP adv.,*2013, **3**, 022126; M. Yin, A. B. Yusov, A. M. Fedosseev and J. C. Krupa, *J. Phys.: Condens. Matter* 2002, **14**, 8743.

20 S. Surviliene, O. Nivinskiene, A. Cesuniene and A. Selskis, *J. Appl. Electrochem*., 2006, **36**, 649.

21 O. Kahn, *Molecular Magnetism*; VCH Publishers: Weinheim, Germany,1993; p 47.

22 A. M. Atria, R. Baggio, M. T. Garland, J. C. Munoz and O. Pena, *Inor. Chim. Acta,* 2004, **357***,* 1997; H. An, D. Xiao, E. Wang, Y. Li, X. Wang and L. Xu, *Eur. J. Inorg. Chem.,* 2005, **854**; J. Li, X. Yu, H. Wang, K. Xu, X. Wu, L. Hou and J. Li, *Trans. Metal Chem.,* 2006, **31**, 770; S. Decurtins, M. Gross, H. W. Schmalle, and S. Ferlay, *Inorg. Chem.* 1998, **37***,* 2443.

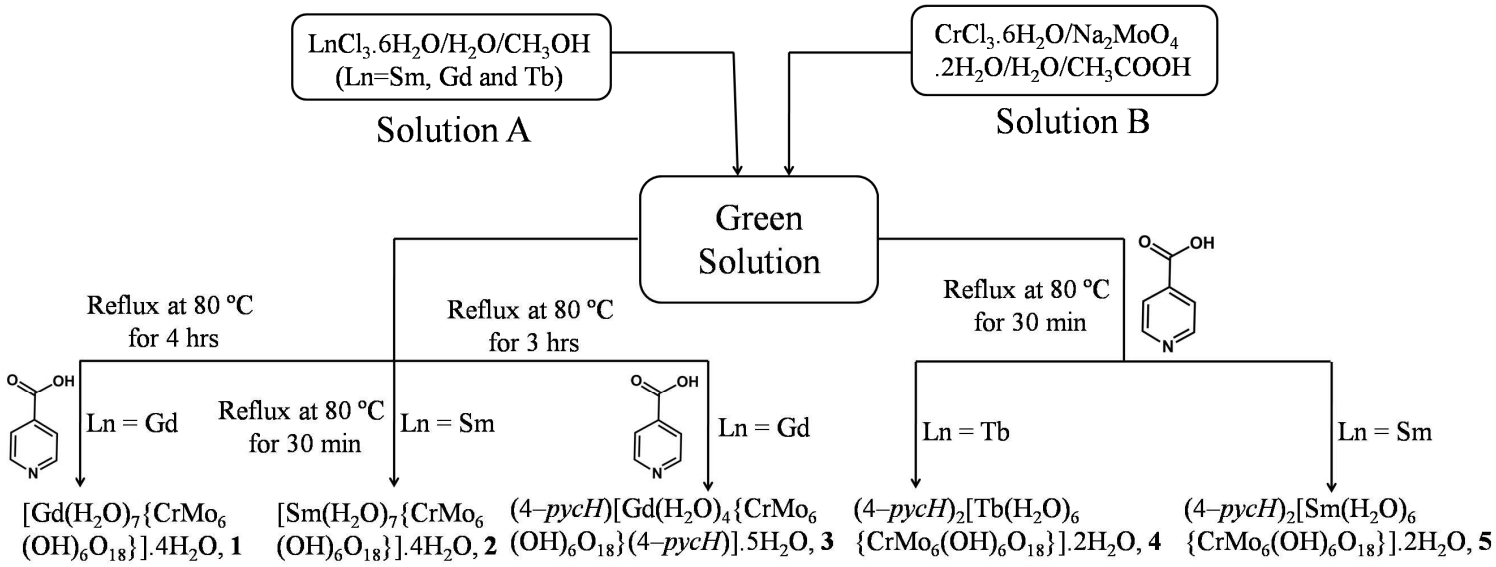

Scheme 1. Synthetic protocol for the crystallization of chromium moybdate based solids **1**–**5**.

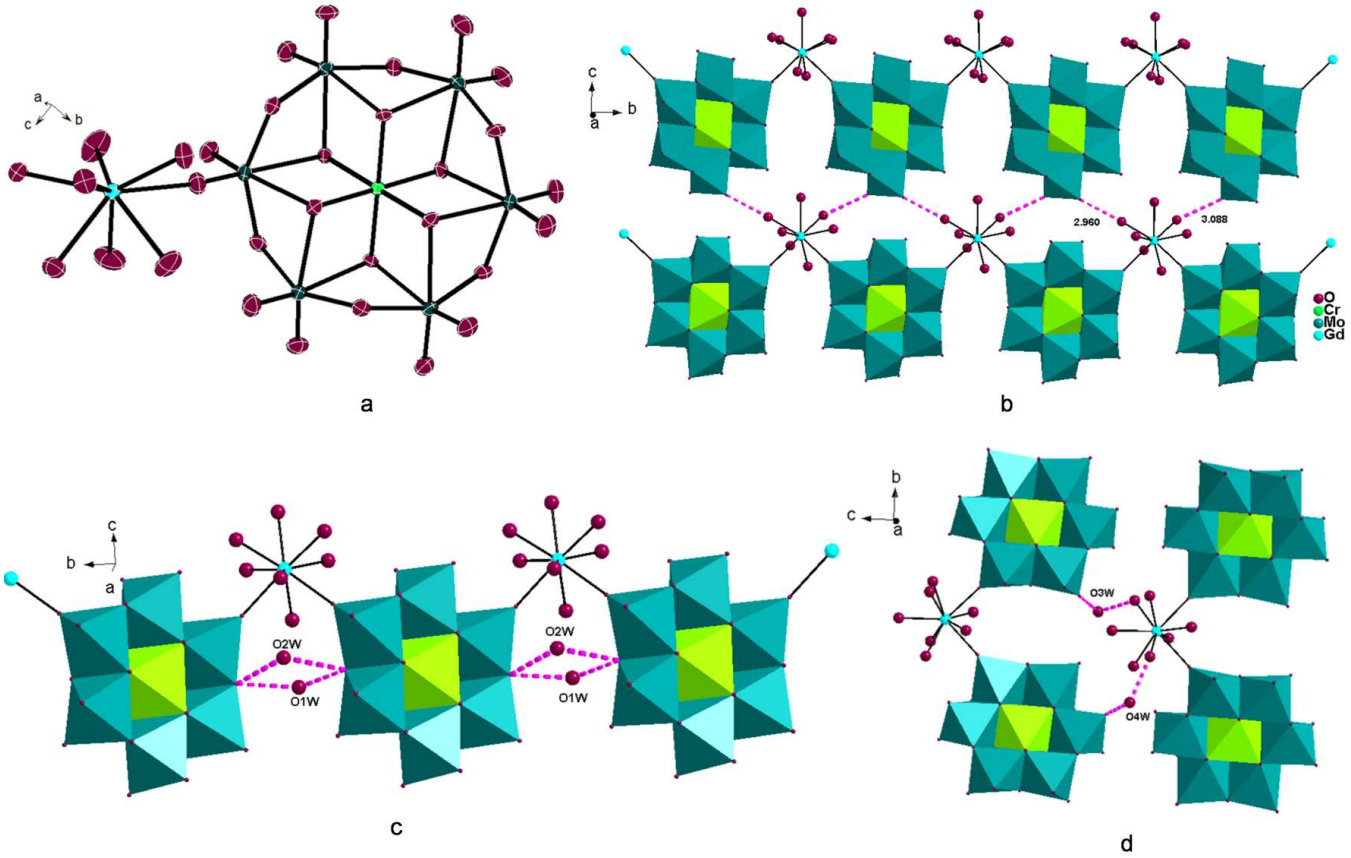

Fig. 1 (a) ORTEP view of asymmetric unit of solid **1**. Thermal ellipsoids are drawn at 50% probability level. (b) In **1** gadolinium atoms are coordinated through chromium molybdate clusters forming 1-D chains. H–bonding between water molecules coordinated to Gd atoms and cluster oxygen result in the formation of 2-D supramolecular sheets on the *bc* plane. Other atoms are omitted for clarity. (c) A pair of lattice water molecules connects the 1-D chains through H–bonding. (d) 2-D supramolecular sheet through H–bonding with water molecules.

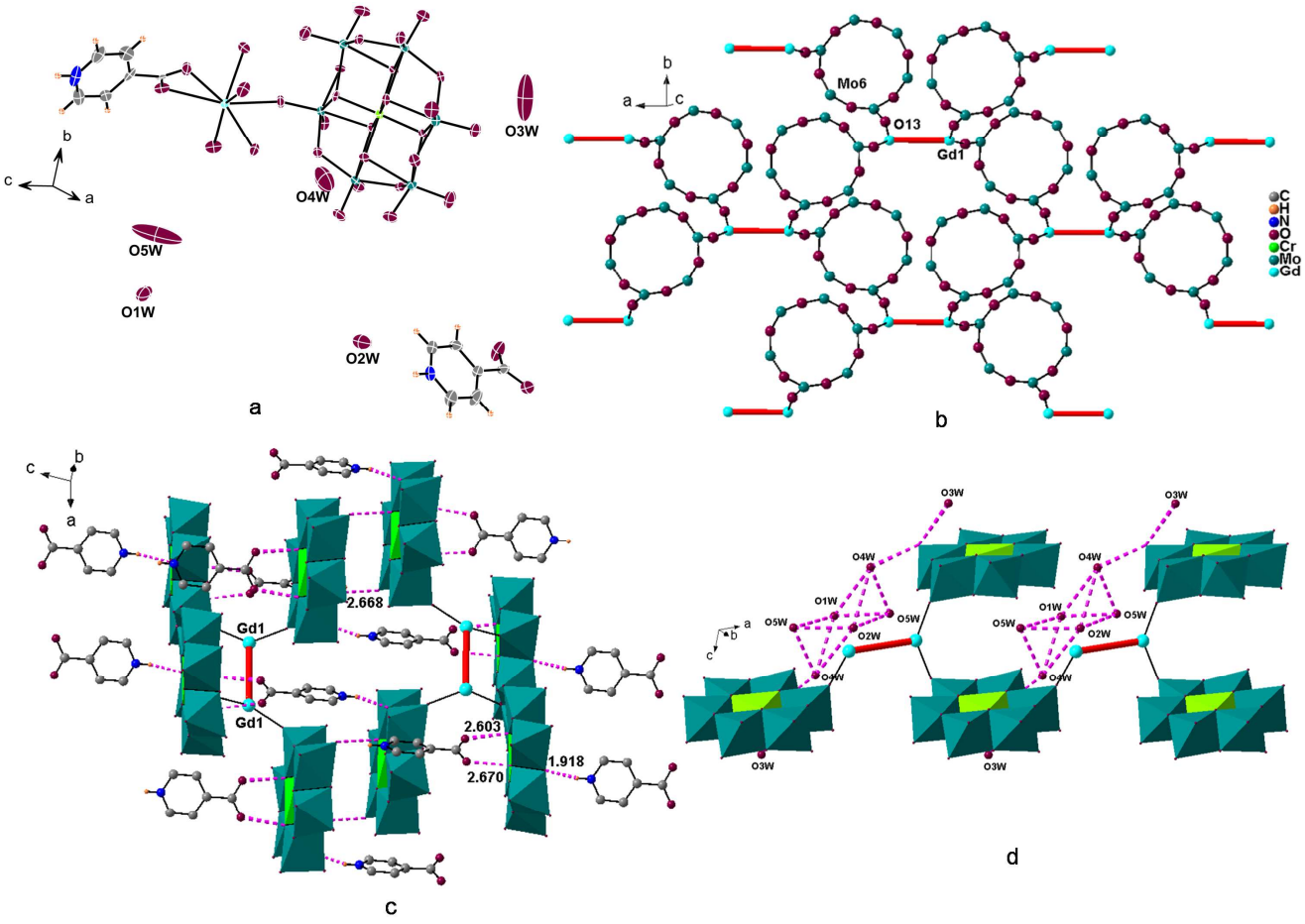

Fig. 2 (a) ORTEP view of asymmetric unit of solid **3**. Thermal ellipsoids are drawn at 50% probability level. (b) 2-D supramolecular sheet of **3** viewed along *ab* plane. Each Gd dimer is coordinated through four POM clusters and each cluster is linked to two Gd atoms forming double stranded sheets. The organic molecules bridging the Gd dimer are omitted for clarity. (c) The zwitterionic organic molecules are locked in between the sheets through H–bonding. (d) A hexameric water cluster in the cavities between the sheets H–bonded to the cluster.

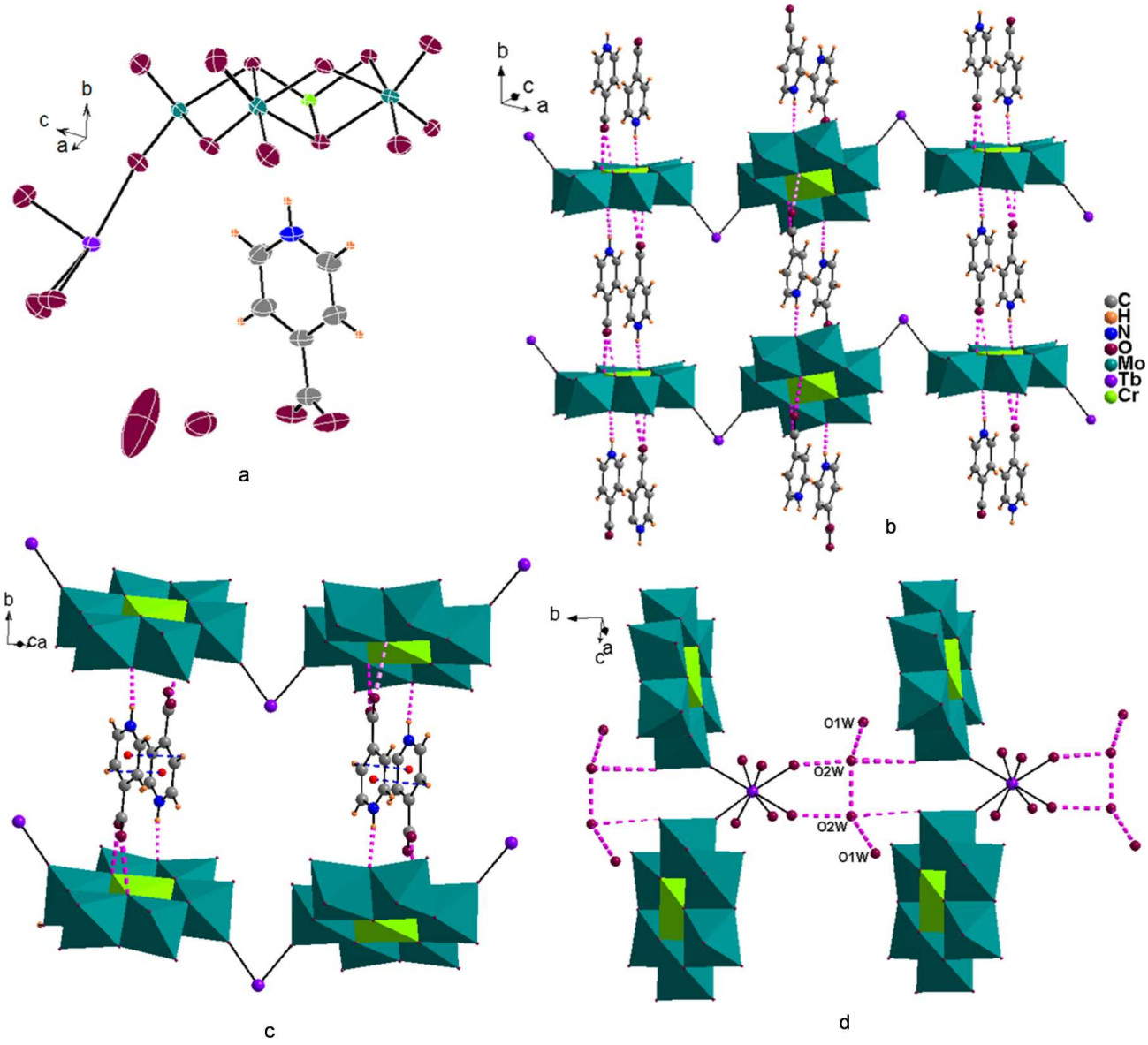

Fig. 3 (a) ORTEP view of asymmetric unit of solid **4**. Thermal ellipsoids are drawn at 50% probability level. (b) Tb atoms link the clusters to form 1-D chains which are further H–bonded (N─H···Ot─Mo and O─H···O─C) to each other through the organic cations. (c) C─H···л interaction between a pair of zwitterionic organic species. (d) A pair of 1-D chains are connected through H–bonding with water molecules.

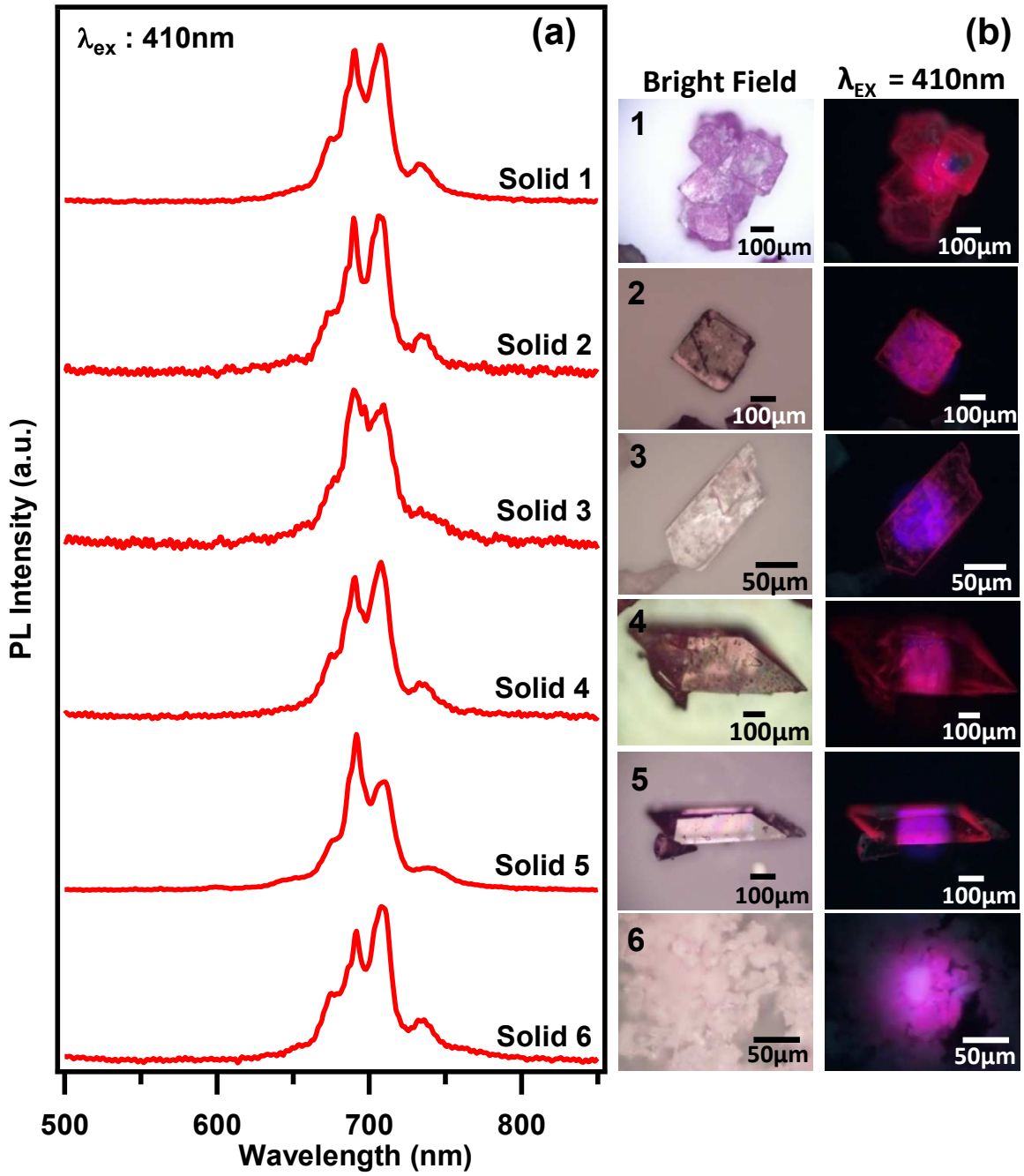

Fig. 4 The room–temperature (a) emission spectra (λ_{ex}~410nm) of crystals **1–6** and corresponding (b) confocal microscopic white light (bright field) reflection and PL images (λ_{ex}~410nm) of the solids **1–6**.

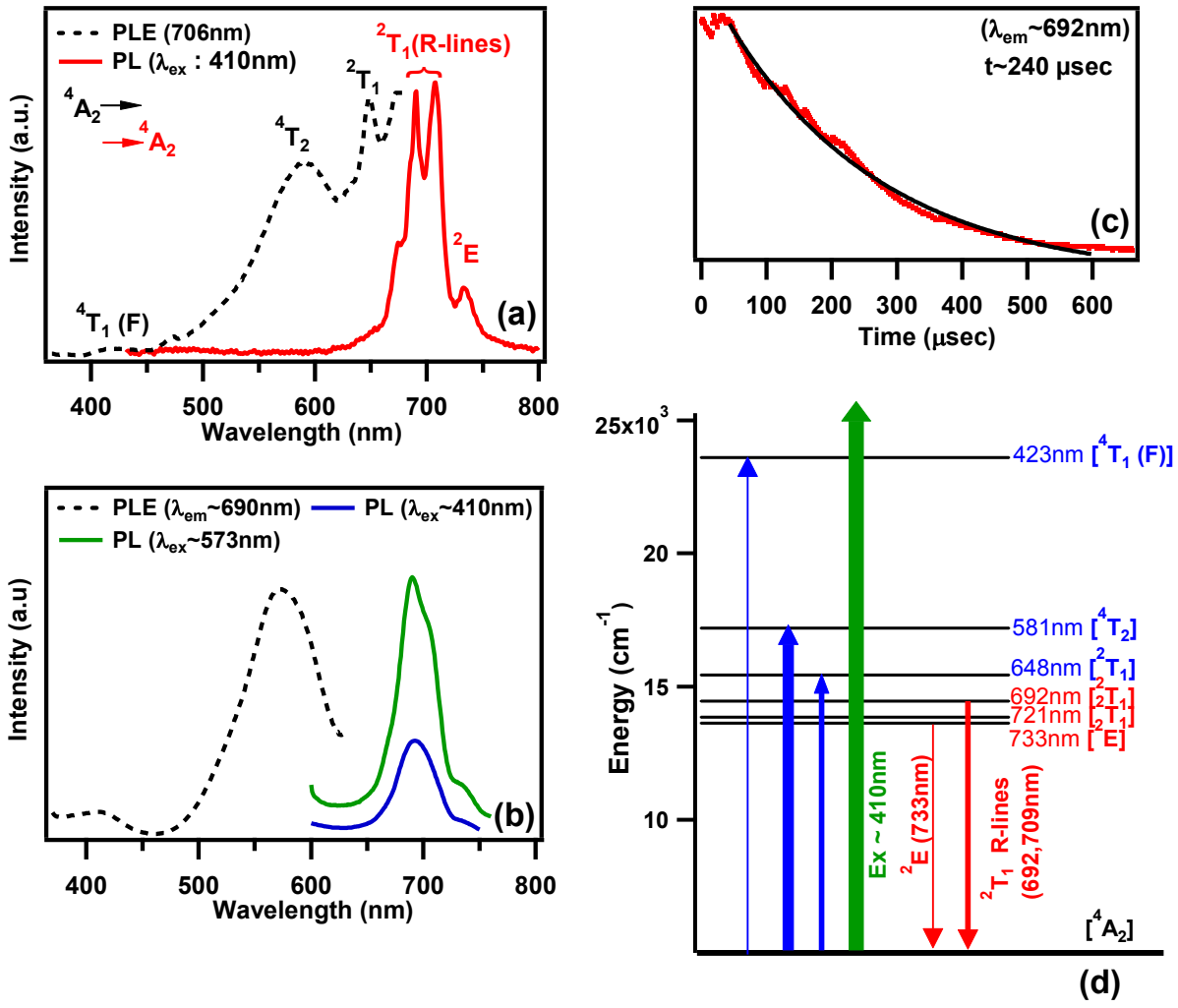

Fig. 5 (a) Room–temperature photoluminescence excitation (PLE) (λ_{em}~706nm) and photoluminescence (PL) spectra (λ_{ex}~410nm) of crystal **5**. (b) Room–temperature PLE (λ_{em}~690nm) and PL spectra (λ_{ex}~410nm, 573nm) of aqueous solution of solid **6** is given for reference. (c) The PL decay curve for λ_{em} = 692nm ($^2T_1 \rightarrow {}^4A_2$ of Cr^{3+}) emission in Cr–doped molybdate (solid **5**). (d) Schematic energy level scheme for Cr^{3+} ion depicting possible internal processes leading to the measurements presented above. (Blue and red colors indicate the absorption and emission transition/levels respectively. Broad green color arrow indicates the laser excitation)

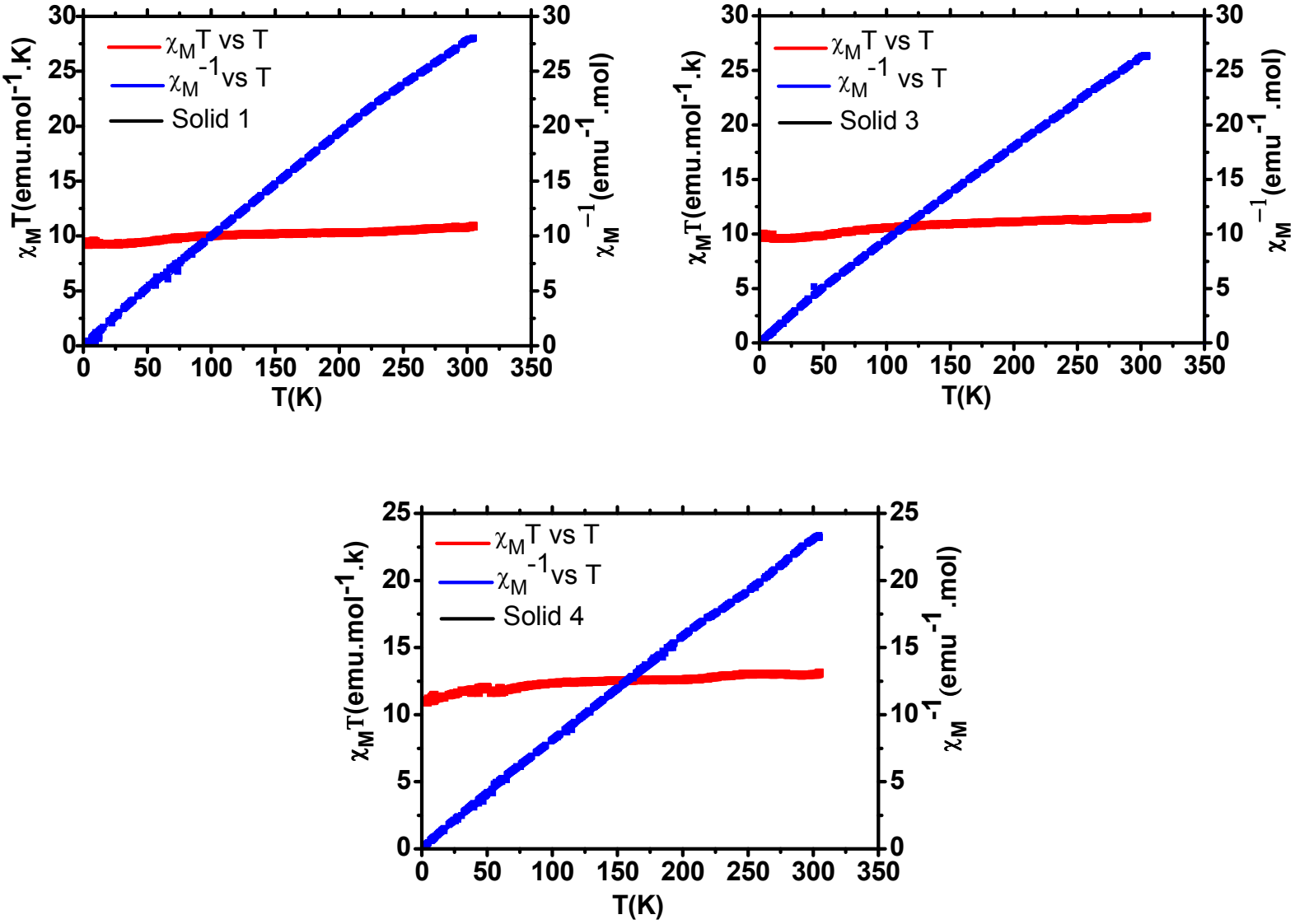

Fig. 6 Plots of $\chi_M T$ and χ_M^{-1} with T for solids **1**, **3** and **4**.

Table 1. Crystallographic and structural refinement for solids **1** and **3–5**.

Parameter	**1**	**3**	**4**	**5**
Formula	$Gd_4Cr_4Mo_{24}O_{140}$	$GdC_{12}H_{10}CrMo_6N_2O_{36}$	$TbC_{12}H_{10}CrMo_6N_2O_{38}$	$SmC_{12}H_{10}CrMo_6N_2O_{38}$
Formula weight	5378.28	1543.11	1576.79	1568.22
T(K)	298(2)	298(2)	298(2)	298(2)
Crystal system	Orthorhombic	Monoclinic	Monoclinic	Monoclinic
Space group	*Pca*2$_1$	*C*2/*c*	*C*2/*c*	*C*2/*c*
a (Å)	11.7941(17)	23.459(7)	18.389(2)	18.4316(14)
b (Å)	10.9501(16)	13.337(4)	12.5427(14)	12.5601(10)
c (Å)	22.359(3)	24.725(8)	17.963(2)	17.9491(14)
α (°)	90.00	90.00	90.00	90.00
β (°)	90.00	102.957(5)	104.117(2)	104.117(2)
γ (°)	90.00	90.0	90.00	90.00
V (Å^3)	2887.6(7)	7539(4)	4018.0(8)	4026.5(5)
Z	1	8	4	4
D_{calc}, (g cm^{-3})	3.093	2.719	2.607	2.587
$\mu_{MoK\alpha}$ (cm^{-1})	5.266	4.057	3.922	3.616
λ (Å)	0.71073	0.71073	0.71073	0.71073
Theta Range,°	2.25– 28.15	2.30– 28.28	2.44–28.30	2.34–28.02
No. measured reflections	26204	35202	10273	8138
No. unique reflections	5150	6637	3533	3547
No. refined parameters	390	524	273	273
R_1, wR_2 [I	0.0284, 0.0648	0.0635, 0.1202	0.0313, 0.0972	0.0323, 0.0810

$> 2\sigma(I)]$[a]				
Goodness–of–fit (GOF) on F^2	1.190	1.322	1.297	1.040
CCDC no.	922305	806605	940074	946456

Table 2. Calculated and observed values of the product of the molar Magnetic Susceptibility χ_M and the temperature for compounds **1**, **3** and **4**.

Solid Ln-Cr	$\chi_M T$ **(cal.) (300K) (emu. mol^{-1}.K)**	$\chi_M T$ **(obs.) (300K) (emu. mol^{-1}.K)**
1 (Gd^{3+})	9.75	9.93
3 (Gd^{3+})	9.75	10.55
4 (Tb^{3+})	13.68	12.15